Performance of GPR attribute analysis to detect and characterise buried archaeological targets near Ukhaidir palace, Iraq

Z.T. Abdulrazzaq[1], J.M. Thabit[2] and A.J. Al-Khafaji[3]

[1] Directorate of Space and Communications, Ministry of Science and Technology, Baghdad, Iraq
[2] Department of Geology, College of Science, University of Baghdad, Iraq
[3] Department of Oil Engineering, College of Engineering, University of Karbala, Iraq

ABSTRACT   Ukhaidir palace is an outstanding example of Mesopotamian architecture and of great interest to many researchers and archaeologists. However, the builder of this palace and the time of construction remain controversial. During recent decades, several archaeological sites and cultural heritage around it have vanished as a result of neglect, degradation, and man-made interventions. A ground penetrating radar (GPR) survey was conducted at two sites (A and B) near the palace: site A is located in front of the palace a few metres away, while site B is located about 155 m NE of the palace. 2D and 3D GPR attribute analysis were used, including the instantaneous phase, root-mean-square (RMS) amplitude, as well as sweetness attributes to improve the interpretation and achieve the best results. The results led to identifying a number of anomalies: seven of them were interpreted to be ancient walls, while the others were associated with a *karez* (water canal) and an external wall. RMS amplitude and sweetness attributes successfully determined the boundaries and the horizontal continuity of the ancient walls, but the RMS amplitude was more accurate. The instantaneous phase detected the highly contrasting features of the buried structures but failed to specify the targets having an angle equal or close to the soil phase angle.

Key words: 3D GPR, *karez*, attributes analysis, Wadi Al-Abyadh, archaeological structures.

1. Introduction

During recent decades, archaeological geophysics has gained enormous popularity within the archaeological community. Ground penetrating radar (GPR) is one of the high-resolution geophysical exploration methods that uses electromagnetic (EM) waves to image and characterise near-surface buried targets (Davis and Annan, 1989). However, to produce reflections and refractions from buried targets, there must be sufficient contrasts of EM impedance during the wave propagation within the Earth. The major goal of the GPR survey is to map archaeological features. As the signal velocity is a known value, the distance can be calculated accurately by measuring the time taken by the signal to travel in the subsurface (Conyers and Goodman, 1997). Nonetheless, prospecting for archaeological features is different from treasure hunting; it requires knowing more quantitative information about these features, such as the geometry,

shape, size, depth of the objects, and other characteristics from the surveys (Zhao *et al.*, 2012).

The methodology for acquiring and interpreting GPR data is very similar to that of the more consolidated geophysical exploration method of seismic reflection. Both methods use the reflection of energy from underground structures but they differ greatly in the site-specific application (Sharma, 1997). Despite the accuracy of GPR in identifying buried objects, there is considerable ambiguity in its interpretation of complex sites, especially archaeological sites. Accordingly, many researchers have tended to use the advanced analysis of seismic data, known as "seismic attributes analysis", on GPR data to improve the interpretation, and to obtain the best results. Böniger and Tronicke (2010) employed similarity, energy, and coherency attributes to analyse the 3D GPR data to localise and characterise the tombs inside medieval chapels in the state of Brandenburg, Germany. The results demonstrated the superior interpretability of these attributes in the identification and characterisation of the tombs compared with the 3D modern visualisation techniques. Zhao *et al.* (2012) applied many GPR attribute analyses, including root-mean-square (RMS) amplitude, maximum peak time, average peak amplitude, and instantaneous phase, to extract and describe different archaeological targets (ancient kiln site, ancient wall, and tomb) in the ancient Nanzhao castle site. The results clarified that the use of different attribute analyses is better than the results based on a time slice. Khwanmuang and Udphuay (2012) evaluated three types of attribute analyses, including steepness event, instantaneous-amplitude, and energy attributes, to improve visualisation and associated interpretation for archaeological targets of an old pagoda in Chiang Mai city, Thailand. The attribute analysis provided clearer images of the edge of buried archaeological structures than GPR data with traditional processing. However, no study has been conducted yet on the use of GPR attribute techniques for improving the archaeological interpretations in Iraq.

The data of EM methods are sensitive to variations in the electrical properties of the medium. The forward and inverse modelling of 2D and 3D can reconstruct distributions of permittivity and conductivity. Lambot *et al.* (2004) developed a new approach by integrated forward and inversion modelling of the GPR signal to estimate the dielectric permittivity and electric conductivity of the shallow subsurface, and the approach was validated under laboratory conditions on homogeneous sand subject to different water contents. Lavoue (2014) developed a quantitative imaging method for the reconstruction of 2D distributions of permittivity and conductivity from GPR data acquired from the ground surface. The method employs the full waveform inversion (FWI) technique, originating from seismic exploration, which exploits the entire recorded radargrams and has proved successful in crosshole GPR applications. Furthermore, the finite-difference and finite-element methods are used to predict the EM response correctly, after solving Maxwell's equations, taking into account the physical and geometrical properties of the considered problem and its initial conditions (Pajewski *et al.*, 2015). These methods are usually used to solve a problem of 3D EM modelling based on 2.5D EM (Li *et al.*, 2017), and are amply studied in former publications (e.g. Li and Pek, 2008; Li *et al.*, 2020).

Seismic and GPR techniques are radically different concerning energy sources and measured physical parameters, though the data processing and interpretation techniques have many similarities (Zhao *et al.*, 2013). The aim of this research is to enhance the signal characteristics of GPR data by using multi attribute analysis for the identification and characterisation of the archaeological targets.

2. Site description

Ukhaidir palace is the name of the enormous ancient fortress still standing today in a historically significant location in Iraq western desert, situated between latitude of 32° 25' to 32° 26' north, and longitude of 43° 35' to 43° 36' east, as shown in Fig. 1. The palace, considered one of the greatest testimonies of Islamic architecture, was built as a defensive fortress located 35 km SW of the city of Karbala and around 192 km SW of Baghdad (Abdulrazzaq *et al.*, 2019). The estimated date of the construction of the fortress is between 720 and 800 A.D. (Creswell, 1958), most likely in the era of second Abbasid caliph Al Mansoor Billah (Al-Hussaini, 1966). The climate of the study area is considered an arid climate (desert climate), with cold dry winters and hot dry summers (Alwan *et al.*, 2019), and an average precipitation ranging between 100 to 150 mm (Abdulrazzaq, 2020). Topographically, the area surrounding the palace is located at a height of 38 m above sea level, surrounded by a simple topography, with gently sloping terrain oriented to the NE towards Wadi Al-Abyadh. Geologically, the age of the numerous formations in the surroundings of the study area range from Tertiary rocks to the Quaternary deposits. Recent deposits cover most of the area. In particular, Gypcrete sediments spread out over large parts of the area. They are result of erosion processes on carbon stones/rocks of Triassic and before (Al-Jiburi and Al-Basrawi, 2002).

Ukhaidir palace is one of the most complex archaeological sites that have witnessed multiple eras. Reuther (1912) wrote about the construction of the palace and reported that several defensive installations, that were not included in the construction plan, had been added, especially at the
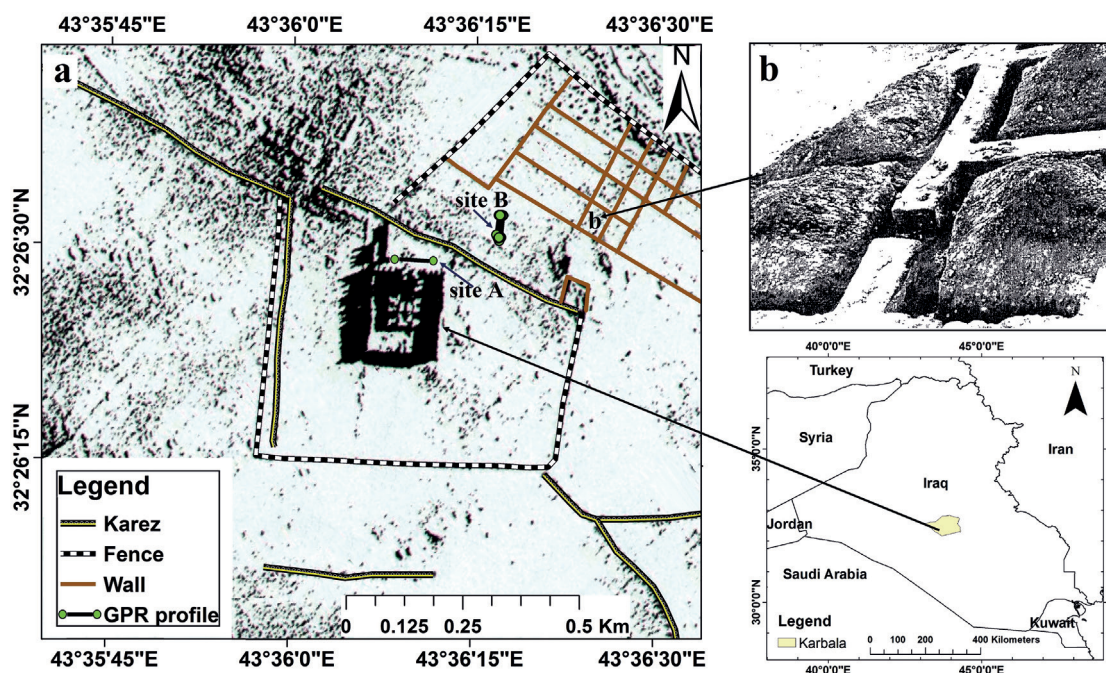

Fig. 1 - The location of Ukhaidir palace: a) an aerial photograph showing the internal and external walls (fence), dwelling houses and *karezes* (after G.C.S., 1935; Al-Janabi, 1977); b) a photograph showing the rooms and facilities built of bricks east and NE the fortress (Al-Janabi, 1977).

main entrance. This included the extension of the walls and the widening of the doors, which transformed it from a palace to a fortress. An aerial photograph of the Ukhaidir site was taken in 1935, which represented the internal and external walls and many dwelling houses (Fig. 1a); it also revealed the presence of many *karezes* (water canals) around the fortress. *Karez* is a system of water supply made with stone roof supports (Fig. 2) consisting of subsurface tunnels with a gradual slope, engineered to collect groundwater from mountainous or flat regions and able to deliver large quantities of water without the need for pumping (Lightfoot, 2009). These *karezes* were used by the human settlements that lived near the palace to collect rainwater and utilise it for agricultural and domestic use. Al-Janabi (1977) excavated several building units and facilities built of bricks in the form of rooms with different sizes (Fig. 1b) NE of the palace. Accordingly, we expect the presence of several archaeological structures buried in front of the palace and surrounding it.

Fig. 2 - Photographs showing examples of *karezes* design in Iraq: a) round arch *karez* tunnel in limestone at Zimzimuk (Lightfoot, 2009), b) *karez* tunnel in limestone at Sulaimaniyah city (Al-Manmi *et al.*, 2019).

3. Materials and methods

3.1. The fundamentals of GPR

The success of GPR surveys depends on variable EM properties of Earth materials (soil and sediment mineralogy, clay content, ground moisture), which affect the capacity and speed of the EM energy propagation through a material, and the attenuation of EM energy after it is transmitted. The depth of penetration of the EM wave and the GPR system is dependent on the frequency of the system's transmitting antenna. Higher radar antenna frequencies cannot penetrate the subsurface to the same extent as lower frequency antennas. However, along with the greater penetration depths achievable with lower frequency units comes lower spatial resolution (Conyers and Goodman, 1997).

The most important physical conditions, which influence the behaviour of radar waves in the medium, are electrical conductivity (σ), dielectric permittivity (ε) and magnetic permeability (μ) (Annan, 2009). Electrical conductivity can greatly affect the energy loss or attenuation of the EM signal, which in turn governs signal penetration depth, where a high conductivity will attenuate

GPR signals rapidly (Davis and Annan, 1989). Dielectric permittivity, in simple terms, is the ability of the material to hold an electrical charge. The dielectric permittivity of free space is considered as a reference material, which is equal to $\varepsilon_o = 8.854 \times 10^{-9}$ F/m. Permittivity of different materials is expressed as a ratio to ε_o, called Relative Dielectric Permittivity (RDP), also called the dielectric constant (ε_r). RDP is usually determined empirically from measurements in the field but can be directly measured in laboratory (Annan, 2009). Magnetic permeability describes how intrinsic atomic and molecular magnetic moments respond to a magnetic field (i.e. μ represents the relation between the magnetic moments and the magnetic field). It is referred to the capacity of a material to become magnetised as it is introduced to an EM field. Magnetic permeability also affects radar penetration in a medium. Sometimes the relative magnetic permeability is used, which is equal to the magnetic permeability of a material divided by the magnetic permeability of vacuum ($\mu_0 = 4\pi \times 10^{-7}$ H/m). Nevertheless, most soils and sediments are only slightly magnetic and, therefore, have a low magnetic permeability; hence, it is less important than electric conductivity and relative permittivity with regard to wave propagation (Baker *et al.,* 2007).

3.2. Data measuring and processing

MALÅ RAMAC/GPR system (Malå, 2005) was used in this study with a 250 MHz shielded antenna to detect and characterise the buried cultural heritage remains in front of and near Ukhaidir palace. The 250 MHz antenna was selected for being more suitable than a 400 MHz antenna to detect the archaeological structures at depths ranging between 1-10 m, as well as to mitigate the potentially negative effects of the lossy substrate (Urban *et al.*, 2014; Andreou *et al.*, 2017). The GPR survey profiles were orientated approximately perpendicular to the expected archaeological structures. The survey included two sites; site A was in front of the palace, a few metres away. Two parallel profiles in this site were measured in a W-E direction, with a distance of 5 m separating the profiles. The length of each profile was 100 m. Site B is located about 155 m NE of Ukhaidir palace (Fig. 1a). Nine parallel GPR profiles were carried out on this site. Each profile was 42.5 m long with 1 m distance between the profiles, covering an area of 9.0×42.5 m^2. The values of the operating parameters of the survey were:

1. sampling frequency: 2500 MHz;
2. sampling interval: 0.2 ns;
3. antenna spacing: 0.18 m;
4. velocity: 0.1 m/ns;
5. time windows: 102 ns.

The sampling frequency was 2500 MHz, simply set to approximately 10 times the antenna frequency used (MALÅ, 2005). All GPR profiles were collected with an antenna spacing of 0.18 m, and 0.2 ns sampling interval to avoid spatial aliasing. The velocity (0.1 m/ns) was chosen according to previous studies (e.g. Al-Khersan *et al.*, 2016; Nehaba *et al.*, 2019) conducted with similar substrate conditions and similar building materials to those found at Ukhaidir palace. The time window was set at 102 ns, assuming that the archaeological structures are located at a depth range of 0.1 to 3.0 m below the surface.

The GPR row data were processed using Reflex-Win v.7.2 (Sandmeier, 2008) utilising the common filters, including subtract mean (dewow), static correction, background removal, manual gain (*y*), and band base filter, respectively. The subtract mean (dewow) filter was used to eliminate direct current (DC) bias in data and may be used for eliminating a possible low frequency part

(dewow) (Cassidy, 2009). Static correction was used to adjust the zero time; background removal was used to remove horizontal or almost horizontal features from GPR data and allows subtle weaker signals to become visible in the processed section (Parkin *et al.*, 2000); *y* was used to maximally equalise the radar signals, and band base filter to remove unwanted frequencies from the traces. This sequence may be regarded as a standard for GPR data (Sandmeier, 2008). After applying these filters, 2D GPR data were exported as SEG-Y format and imported into the Petrel v.2015.5 software (Schlumberger, 2016) for the application of attribute analysis.

3.3. 3D GPR geometry

In spite of the availability of many 3D data visualisation techniques associated with interpretation such as isosurfaces, time-slices, and 3D cube, in complex subsurface cases, these techniques may be not appropriate (Conyers and Goodman, 1997). Attribute analysis is considered one solution for enhanced complexity of GPR data interpretations compared with the traditional techniques (Khwanmuang and Udphuay, 2012; Zhao *et al.*, 2013).

A typical 3D GPR data file acquisition is a grid of closely spaced lines; crossing each other and provided by highly dense sampling measurements of the underground reflectivity. Each GPR trace is characterised by the corresponding positions of the transmitter and receiver antenna. The coordinates of the transmitter and receiver antenna are defined according to a preferably orthogonal coordinate system. The so-called in-line is a GPR line parallel to the X-axis direction in which the data is recorded, while the line recorded parallel to the Y-axis direction and perpendicular to the in-line is commonly referred to as a cross-line (Ahmed, 2015).

In 3D, the midpoint and half-offset coordinates are vectors, whereas, in 2D, they reduce to scalars. The azimuth is the angle between the vertical projection of a line of interest and true north. If the transmitter and receiver are aligned along one direction, it is assumed that the X-axis is aligned with this direction. In this case, most of the offsets are distributed in a narrow range of azimuth (Biondi, 2006).

A 3D simple grid is generated from a 2D GPR frame that includes top, bottom, and azimuth boundaries (Fig. 3a). The top represents the time zero, while the bottom is equal to the residual time window, where the azimuth represents the survey direction. The workflow is filled by in-lines and cross-lines. The 100 in-lines and 500 cross-lines are distributed towards 7.14 degree NE azimuth direction. The generated 3D cube will be populated with GPR attributes from the 2D profiles. Subsequently, the undefined values between the GPR data will be filled by using the kriging algorithm (Fig. 3b).

3.4. Attribute analysis

An attribute analysis is defined as information (calculated using Hilbert transform), such as time, amplitude, and phase, which may be extracted or derived from the raw data (Chopra and Marfurt, 2005). Attribute analysis technology application on seismic data began during the search for hydrocarbon in rock pores (bright spots) in the early 1970s. In the meantime, with the continued development of multiple types of seismic attributes analysis, several attempts were made to classify them into categories for implementation in the hydrocarbon exploration field (Vohs, 2016). In general, seismic attributes are kinematic, geometric, dynamic, and statistical features derived from seismic data (Taner, 2001). Economou *et al.* (2015) classified GPR attributes into five main categories including geometrical statistical attributes, instantaneous attributes, texture
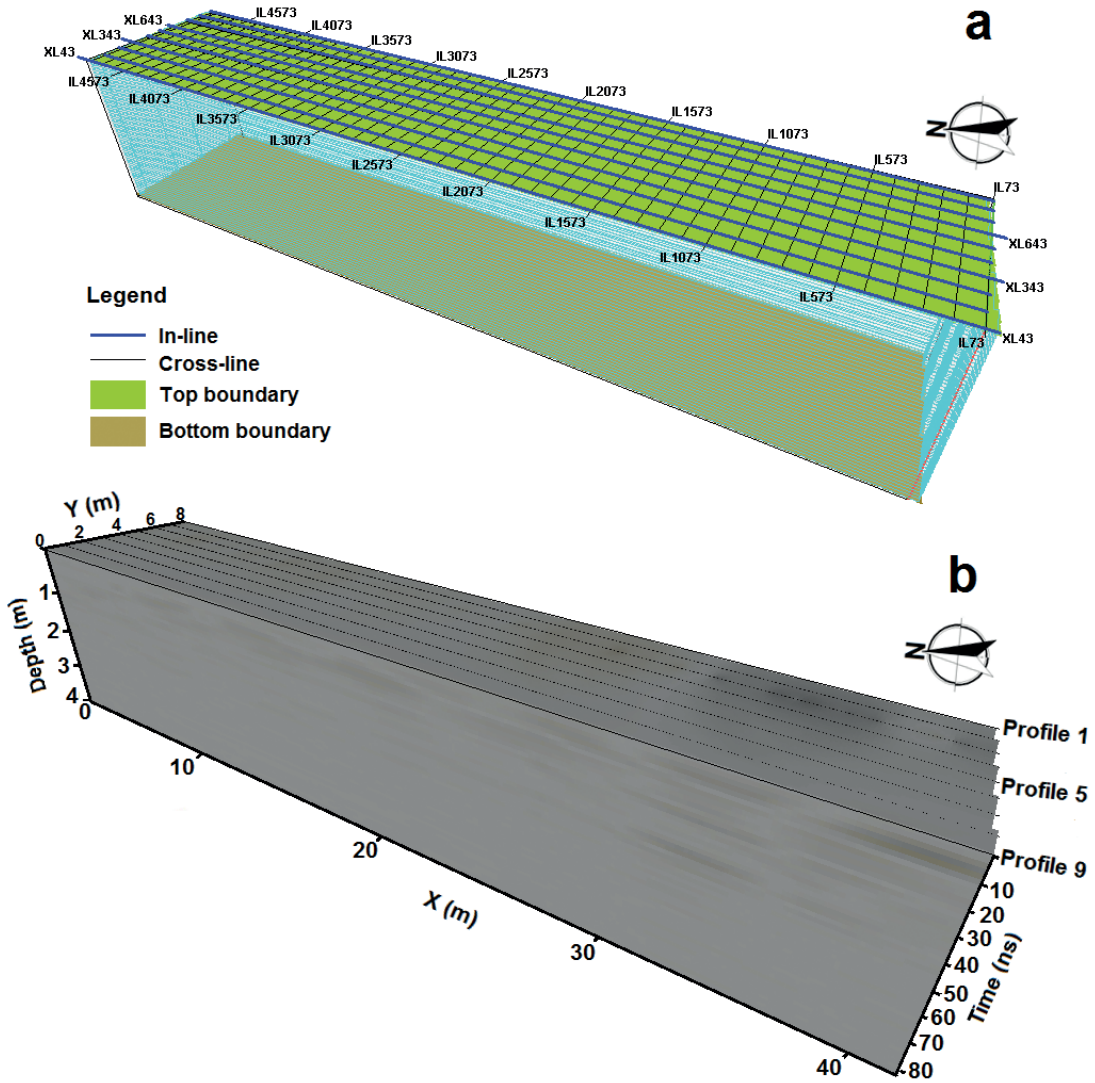
Fig. 3 - 3D GPR geometry: a) 3D simple grid that generated from 2D GPR frame; b) 3D cube populated with GPR attributes generated from the 2D profiles.

attributes, coherency-semblance attributes, and wavelet attributes. Here, the most common instantaneous attributes analysis is used, including instantaneous phase, RMS amplitude, and sweetness to enhance GPR signal characteristics.

The instantaneous phase is defined as "the orientation angle of the amplitude vector at a particular time and relates to the propagation phase of the seismic wave front". A wave front is defined as a line of constant phase, which makes the phase attribute a physical attribute that can be used to describe a geometrical shape. It is normally computed by an arc-tangent function and expressed by (Taner *et al*., 1977):

$$\varnothing(t) = \arctan\left(\frac{\text{Im } F(t)}{\text{Re } F(t)}\right). \tag{1}$$

where t is time (or depth), Im $F(t)$ is the imaginary component of the complex trace, and Re $F(t)$ is the real component of the complex seismic or GPR trace.

The continuity of phase during the propagation of EM waves through the medium reflects the homogeneity and isotropy of the properties. Thus, the instantaneous phase can identify faults, bed interfaces, sequence boundaries (dos Reis Jr *et al.*, 2014), and abnormal bodies clearly by significant phase changes (Zhao *et al.*, 2012).

RMS amplitude is an attribute derived from the amplitude information in the seismic or GPR data. It computes the square root of the sum of squared amplitude over a number (n) of samples (specified window) within a time interval, where the number of samples defines a window length parameter, the RMS value is (Sheriff, 2002):

$$R_{rms,n} = \sqrt{\frac{(x_1^2 + x_2^2 + \dots + x_n^2)}{n}} \ . \tag{2}$$

here, n is the number of samples over a chosen time window, x_n is the amplitude value for the nth sample.

The reflection occurs at a boundary between layers of different impedances (Okoli *et al.*, 2018). Amplitude (whether peak or trough) is sensitive to changes in EM impedance and can provide a piece of beneficial information about the relative value of EM impedance of subsurface materials (Chopra and Marfurt, 2005). A high RMS may result either from a high EM impedance contrast of fill sediments with the surrounding lithology or from the EM impedance contrast due to the change in the permittivity caused by the local conditions of the soil, that always has variable chemical constituents, differences in retained moisture, compaction, and porosity (Conyers, 2004).

Sweetness is defined as reflection strength over the square root of instantaneous frequency (*IF*) (Radovich and Oliveros, 1998). This attribute is also known as amplitude envelope (*AE*) or instantaneous amplitude (*IA*). Reflection strength is the amplitude *AE* independent of phase, and *IF* is the rate of change of phase (Hart, 2008). Thus, the formula of sweetness is defined as follows:

$$Sweetness = \frac{AE}{\sqrt{IF}} \ . \tag{3}$$

The sweetness attribute is useful in detecting channels (Hart, 2008; Li *et al.*, 2017), especially in clastic settings, where boundaries with high EM impedance contrast will generate high amplitude on a GPR profile.

4. Results and discussion

Recorded GPR profiles after the primary processing are shown in Fig. 4. These profiles show many shallow reflections. The reflections A, B, D, E, F, and G are probably associated with demolished walls of archaeological structures (Fig. 4). The greater reflections C and H are, instead, probably associated with *karez* and external wall, respectively. In general, the reflections of anomalies in the site A appeared with higher amplitudes than the reflections of site B. This is due to the expected archaeological structures in the site A, probably constructed of stone, while the structures of site B were made of clay brick supported by stones, expect for reflection H.
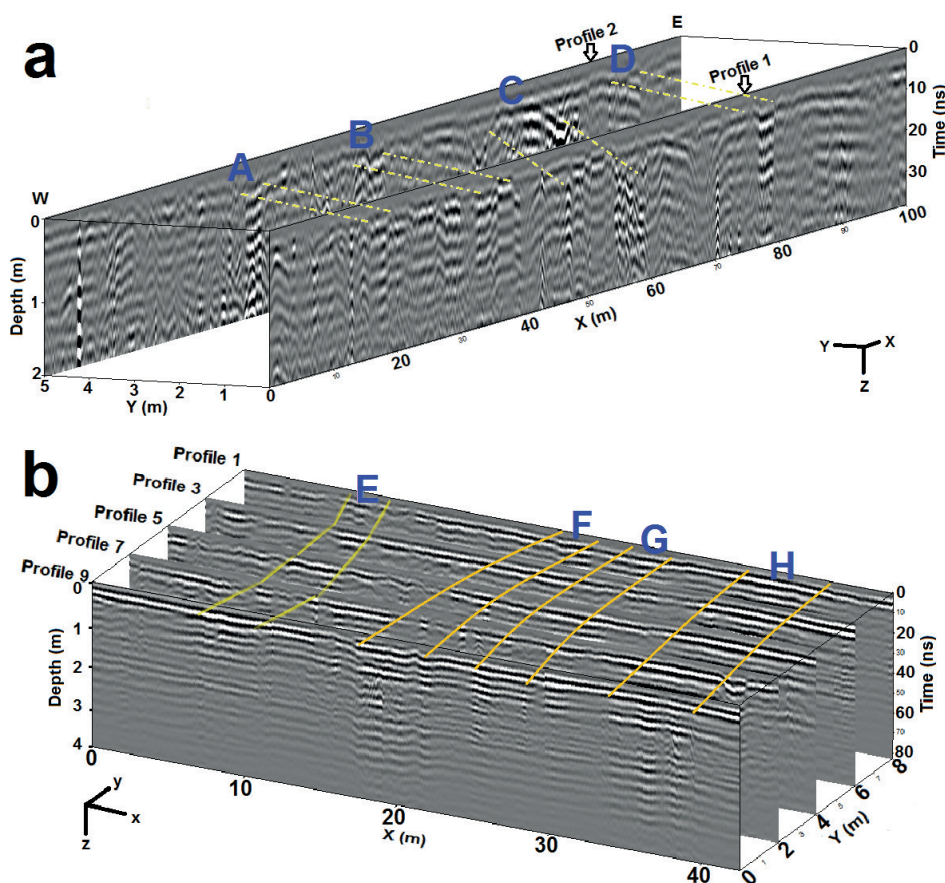
Fig. 4 - The processed 2D profiles show several anomalies: a) profiles of the site A; b) profiles of site B.

The attribute analysis can recognise the subsurface variations in the lithology of strata. However, in archaeology, GPR attributes can indicate the subsurface variations of soil properties. The instantaneous phase, RMS amplitude, and sweetness attributes were calculated after processing the 2D GPR data (site A) and 3D volume data (site B) to improve the overall data interpretation.

4.1. 2D attributes results: survey site A

The GPR profiles of this site show four continuous reflection events over the expected archaeological structures. It was observed that three of these events are strongly indicative of ancient walls, while the fourth event is likely to be a *karez*. Fig. 5 shows the instantaneous phase sections of the GPR profile, which can be helpful to determine the boundaries of the ancient walls by measuring the continuity of these events.

The curvature system of *karez* appears on the RMS amplitude and sweetness attribute profiles, respectively (Figs. 6 and 7). The high amplitude area is interpreted to be limestone-bodies of *karez* while the surrounding low amplitude values are interpreted to be clayey soil. The width of the *karez* is about 8 m, and the depth is about 5 ns time, which corresponds to ~0.25 m. The *karez* is interpreted to be extended laterally and towards the NW of the palace based on its location and morphology in the profiles. The reflections of ancient walls were clearer in RMS amplitude
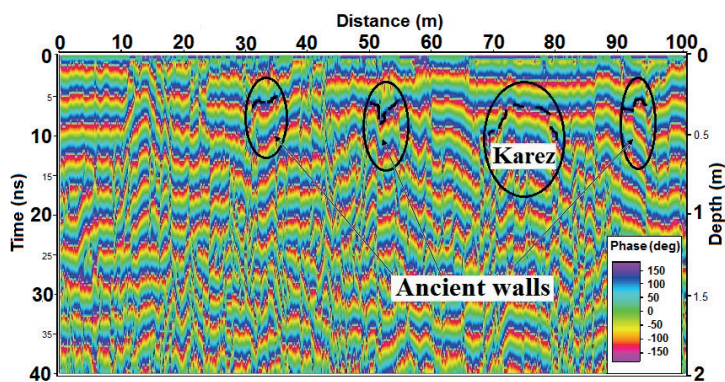
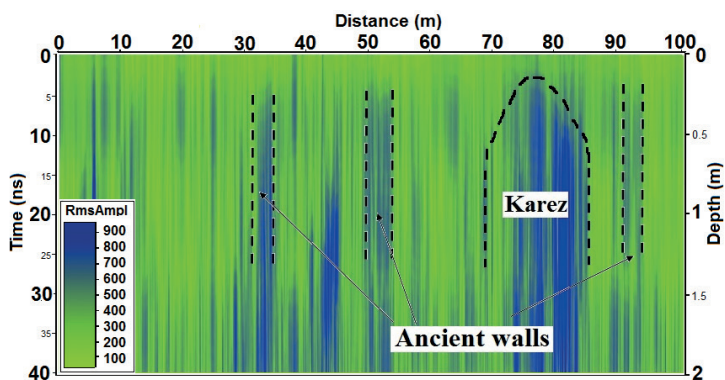Fig. 5 - Instantaneous phase analysis of 2D GPR data (profile 1).

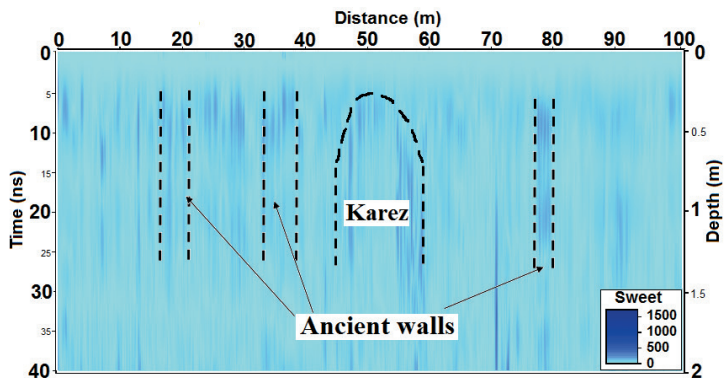Fig. 6 - RMS amplitude analysis of 2D GPR data (profile 1).

Fig. 7 - Sweetness attribute analysis of 2D GPR data (profile 2).

profiles, but in the sweetness attribute profiles, the *karez* boundary is well imaged. The width of the walls ranges between 2 to 3 m with depth of 7 ns time, corresponding to ~0.30 m.

4.2. 3D attributes results: survey site B

The instantaneous phase, RMS amplitude, and sweetness attributes were calculated using a 16-pixel window size. The window size used should be large enough for the mathematical operations to be stable but small enough to provide adequate resolution (Brown, 2011); further, a small window is often used for a shallow objective, and the larger window used for a deeper

objective (Chopra and Marfurt, 2007). Thus, it was preferable to choose an intermediate window size to suppress the noise of the GPR image, as applying a small window may smooth the image too much and result in noisy texture characteristics, whereas increasing windows size tends to increase the anisotropy factor (Eichkitz and Amtmann, 2018). Hence, the choice of the appropriate window size is crucial and depends on the intended application and image resolution. Figs. 8 to 10 present the cross-plots of the instantaneous phase, RMS amplitude, and sweetness attributes, respectively, at 10 ns time corresponding to ~0.50 m below the ground surface with two cross-lines (781 and 565) to represent the horizontal extension of the structures.

The instantaneous phase of the cross-plot (Fig. 8) shows a marked difference in phase of the buried structure in the southern part, associated with a 7-m wide external wall, while no significant change was observed in the remaining parts. The events that did not show up in the cross-plot have a relatively consistent phase angle. The colours in the cross-plot represent various degrees of phase, which relates to the propagation phase of the GPR wavefront. The change in the phase angle near the southern part indicates the lateral continuity of the external wall. The major change in phase angle value around the wall location referred to increasing velocity, which is interpreted as a velocity anomaly associated with increased porosity, and this supports the presence of limestone within the wall components.

The RMS amplitude (Fig. 9) and sweetness attribute (Fig. 10) contain scattered groups of high-amplitude anomalies that may indicate the location of buried archaeological structures interpreted as ancient walls of dwellings (see Fig. 1). The highest-amplitude group is in the southern part of
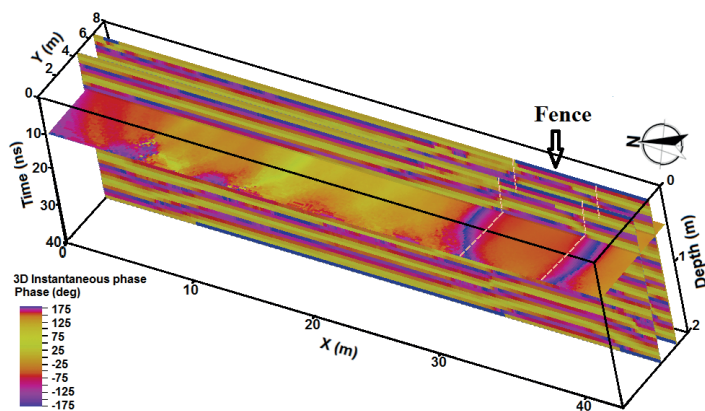

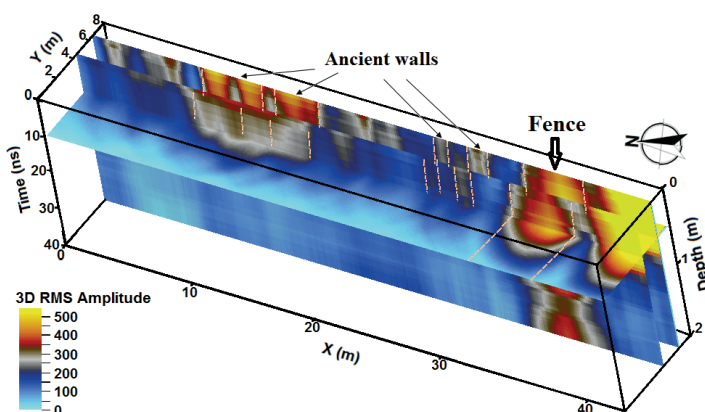Fig. 8 - 3D cross-plot of the instantaneous phase of 3D GPR data.

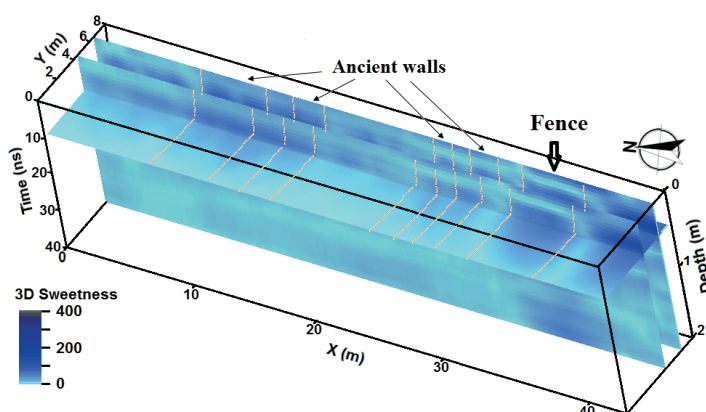Fig. 9 - 3D cross-plot of the RMS amplitude of 3D GPR data.

Fig. 10 - 3D cross-plot of the sweetness attribute of 3D GPR data.

the plots, pointing out a major difference between the materials of this buried structure from its medium as well as from the materials of other expected structures, indicating that the remaining events are associated with clay brick not supported by stones. RMS amplitude determined the boundaries and the horizontal continuity of the ancient walls more accurately than the sweetness attribute. The instantaneous phase failed to specify the targets that have an angle equal or close to the soil phase angle.

5. Conclusions

The main objective of this study was to detect and characterise the buried archaeological structures from the measured GPR data. Using GPR attribute analysis, one *karez*, one external wall, and many ancient walls were identified in the GPR profiles, some of which are not readily interpretable in the raw data. The success of using GPR attributes analysis depends mainly on the value of the dielectric contrast between the targets and their medium. The sweetness attribute was used to image a channel, which is not readily apparent in the raw data and high sweetness attributes are well correlated with the lithology. The results of the study indicate that 2D and 3D GPR attributes can provide more visual and quantitative details of buried archaeological structures, thus improving the quality and efficiency of the GPR interpretation. The visualisation and interpretations of the GPR data acquired at the Ukhaidir site were improved using the instantaneous phase, RMS amplitude, and sweetness attributes. The GPR data with these attributes provide a clearer image of the lateral continuity and the boundaries of buried archaeological structures than the GPR data after common processing steps. RMS amplitude and sweetness attributes mainly provide the continuity of the events on the images, while the instantaneous phase highlights high contrast features. The GPR attribute analysis used in this study is recommended for applications in other investigated archaeological sites.

REFERENCES

Abdulrazzaq Z.T.; 2020: *The feasibility of using TRMM satellite data for missing terrestrial stations in Iraq for mapping the rainfall contour lines*. Civ. Eng. Beyond Limits, **1**, 15-19, doi: 10.36937/cebel.2020.003.003.

Abdulrazzaq Z.T., Thabit J.M. and Al-Khafaji A.J.; 2019: *Identification of archaeological sites threatened with obliteration using space-borne and ground penetrating radars data in site of Tulul al-Ukhaidir, Iraq*. Appl. Geomatics, **11**, 401-412, doi: 10.1007/s12518-019-00272-9.

Ahmed K.A.; 2015: *3-D seismic processing in crystalline rocks using the Common Refection Surface stack*. Ph.D. Thesis in Earth Sciences, University of Hamburg, Hamburg, Germany, 122 pp.

Al-Hussaini M.B.; 1966: *Investigation, maintenance and removal of Debris for the third and fourth seasons*. Sumer, **22**, 79-94.

Al-Janabi K.; 1977: *Archaeological investigations near Ukhaidir*. Sumer, **33**, 119-125.

Al-Jiburi H.K. and Al-Basrawi N.H.; 2002: *Hydrogeological and hydrochemical study of Shithatha Quadrangle (NI-38-13), Scale 1:250000*. GEOSURV, Cronulla, Australia, Internal report No. 2783.

Al-Khersan E.H., Al-Ani J.M.T. and Abrahem S.N.; 2016: *Integrated GPR and ERT as enhanced detection for subsurface historical structures inside Babylonian houses site, Uruk city, southern Iraq*. Pure Appl. Geophys., **173**, 963-982, doi: 10.1007/s00024-015-1162-2.

Al-Manmi D.A., Hamamin D.F. and Salih A.O.; 2019: *Karezes, abandoned and endangered water resources in semi-arid regions: case study from Sulaymaniyah city, Iraq*. Iraqi Bull. Geol. Min., **15**, 91-104.

Alwan I.A., Karim H.H. and Aziz N.A.; 2019: *Agro-Climatic Zones (ACZ) using climate satellite data in Iraq Republic*. IOP Conf. Ser.: Mater. Sci. Eng., **518**, 22-34, doi: 10.1088/1757-899X/518/2/022034.

Andreou G.M., Opitz R., Manning S.W., Fisher K.D., Sewell D.A., Georgiou A. and Urban T.M.; 2017: *Integrated methods for understanding and monitoring the loss of coastal archaeological sites: the case of Tochni - Lakkia, south-central Cyprus*. J. Archaeolog. Sci., **12**, 197-208, doi: 10.1016/j.jasrep.2017.01.025.

Annan A.P.; 2009: *Electromagnetic principles of ground penetrating radar.* In: Jol H.M. (ed), Ground Penetrating Radar Theory and Applications, Elsevier B.V., Amsterdam, The Netherlands, pp. 1-40, doi: 10.1016/B978-0-444-53348-7.00001-6.

Baker G.S., Jordan T.E. and Pardy J.; 2007: *An introduction to ground penetrating radar (GPR)*. In: Baker G.S. and Jol H.M. (eds), Stratigraphic Analyses Using GPR, Geological Society of America, Special Paper 432, pp. 1-18, doi: 10.1130/2007.2432(01).

Biondi B.L.; 2006: *3-D seismic imaging*. Society of Exploration Geophysicists, Tulsa, OK, USA, 247 pp., doi: 10.1190/1.9781560801689.

Böniger U. and Tronicke J.; 2010: *Improving the interpretability of 3D GPR data using target–specific attributes: application to tomb detection*. J. Archaeolog. Sci., **37**, 672-679, doi: 10.1016/j.jas.2009.09.049.

Brown A.R.; 2011: *Interpretation of three-dimensional seismic data*. AAPG Memoir 42, American Association of Petroleum Geologists, Tulsa, OK, USA, 194 pp.

Cassidy N.J.; 2009: *Ground penetrating radar data processing, modelling and analysis*. In: Jol H.M. (ed), Ground Penetrating Radar Theory and Applications, Elsevier B.V., Amsterdam, The Netherlands, pp. 141-172, doi: 10.1016/B978-0-444-53348-7.00005-3.

Chopra S. and Marfurt K.J.; 2005: *Seismic attributes - a historical perspective*. Geophys., **70**, 1-71, doi: 10.1190/1.2098670.

Chopra S. and Marfurt K.J.; 2007: *Seismic attributes for prospect identification and reservoir characterization*. Society of Exploration Geophysicists, Tulsa, OK, USA, 481 pp., doi: 10.1190/1.9781560801900.

Conyers L.B.; 2004: *Ground-penetrating radar for archaeology*. AltaMira Press, Walnut Creek, CA, USA, 205 pp.

Conyers L.B. and Goodman D.; 1997: *Ground penetrating radar: an introduction for archaeologists*. AltaMira Press, London, England, 232 pp.

Creswell K.A.; 1958: *A short account of early Muslim Architecture*. Penguin Books, New York, NY, USA, 330 pp.

Davis J.L. and Annan A.P.; 1989: *Ground-penetrating radar for high resolution mapping of soil and rock stratigraphy*. Geophys. Prospect., **37**, 531-551, doi: 10.1111/j.1365-2478.1989.tb02221.x.

dos Reis Jr J.A., de Castro D.L., de Jesus T.E.S. and Filho F.P.L.; 2014: *Characterization of collapsed paleocave systems using GPR attributes*. J. Appl. Geophys., **103**, 43-56, doi: 10.1016/j.jappgeo.2014.01.007.

Economou N., Vafidis A., Benedetto F. and Alani A.M.; 2015: *GPR data processing techniques*. In: Benedetto A. and Pajewski L. (eds), Civil Engineering Applications of Ground Penetrating Radar, Springer International Publishing, Cham, Switzerland, pp. 281-297, doi: 10.1007/978-3-319-04813-0_11.

Eichkitz C.G. and Amtmann J.; 2018: *GLCM-based anisotropy estimation - the influence of computation parameters on the results*. First Break, **36**, 47-52, doi: 10.3997/1365-2397.n0091.

G.C.S.; 1935: *General Commission for Survey*. Ministry of Water Resources, Iraq.

Hart B.; 2008: *Channel detection in 3-D seismic data using sweetness*. Am. Assoc. Pet. Geol. Bull., **92**, 733-742.

Khwanmuang W. and Udphuay S.; 2012: *Ground-penetrating radar attribute analysis for visualization of subsurface archaeological structures*. The Leading Edge, **31**, 946-949.

Lambot S., Slob E.C., van den Bosch I., Stockbroeckx B. and Vanclooster M.; 2004: *Modeling of ground-penetrating radar for accurate characterization of subsurface electric properties*. IEEE Trans. Geosci. Remote Sens., **42**, 2555-2568, doi: 10.1109/TGRS.2004.834800.

Lavoue F.: 2014: *2D full waveform inversion of ground penetrating radar data: towards multiparameter imaging from surface data*. Ph.D. Thesis in Earth Sciences, University of Grenoble, Grenoble, France, 232 pp.

Li G., Duan S., Cai H., Han B. and Ye Y.; 2020: *An improved interpolation scheme at receiver positions for 2.5D frequency-domain marine controlled-source electromagnetic forward modelling*. Geophys. Prospect., **68**, 1657-1675, doi: 10.1111/1365-2478.12937.

Li Q., Yu S., Wu W., Tong L. and Kang H.; 2017: *Detection of a deep-water channel in 3D seismic data using the sweetness attribute and seismic geomorphology: a case study from the Taranaki Basin, New Zealand*. New Zealand J. Geol. Geophys., **60**, 199-208, doi: 10.1080/00288306.2017.1307230.

Li Y. and Pek J.; 2008: *Adaptive finite element modelling of two-dimensional magnetotelluric fields in general anisotropic media*. Geophys. J. Int., **175**, 942-954, doi: 10.1111/j.1365-246X.2008.03955.x.

Lightfoot D.L.; 2009: *Survey of infiltration karez in northern Iraq: history and current status of underground aqueducts*. UNESCO, Paris, France, Report IQ/2009/SC/RP/1, 56 pp.

MALÅ; 2005: *XV Monitor for ProEx and X3M with Ethernet communication*. MALÅ Geoscience AB, Malå, Sweden, Operating manual v. 1.5, 56 pp.

Nehaba M.S., Thabit J.M. and Mohammed A.J.; 2019: *Using of Ground Penetrating Radar (GPR) for investigate the subsurface archaeological features of Babylon, the ancient city (Mounts zoona)*. Iraqi J. Sci., **60**, 103-114.

Okoli E.A., Onyekuru S.I., Agbasi O.E. and Abdulrazzaq Z.T.; 2018: *Application of model-based inversion technique in a field in the coastal swamp depobelt, Niger Delta*. Int. J. Adv. Geosci., **6**, 122-126, doi: 10.14419/ijag.v6i1.10124.

Pajewski L., Tosti F. and Kusayanagi W.; 2015: *Antennas for GPR systems*. In: Benedetto A. and Pajewski L. (eds), Civil Engineering Applications of Ground Penetrating Radar, Springer International Publishing, Cham, Switzerland, pp. 41-67.

Parkin G., Redman D., von Bertoldi P. and Zhang Z.; 2000: *Measurement of soil water content below a wastewater trench using ground-penetrating radar.* Water Resour. Res., **36**, 2147-2154, doi: 10.1029/2000WR900129.

Radovich B.J. and Oliveros R.B; 1998: *3-D sequence interpretation of seismic instantaneous attributes from the Gorgon field*. The Leading Edge, **17**, 1286-1293, doi: 10.1190/1.1438125.

Reuther O.; 1912: *Ocheïdir: Nach Aufnahmen Von Mitgliedern Der Babylon-Expedition Der Deutschen Orient-Gesellschaft*. J.C. Hinrichs, Leipzig, Germany, 52 pp.

Sandmeier K.J.; 2008: *Reflexw 5.0 manual*. Sandmeier Software, Karlsruhe, Germany, 723 pp.

Schlumberger; 2016: *The Petrel E&P software platform, v2015.5 (64-bit)*, <www.software.slb.com/software-news/support-news/petrel/petrel-2015-5>.

Sharma P.V.; 1997: *Environmental and engineering geophysics*. Cambridge University Press, Cambridge, UK, 500 pp.

Sheriff R.E.; 2002: *Encyclopedic dictionary of applied geophysics, 4th ed*. Society of Exploration Geophysicists, Tulsa, OK, USA, Vol. 13, 442 pp., doi: 10.1190/1.9781560802969.

Taner M.T.; 2001: *Seismic attributes*. Recorder, **26**, 48-56.

Taner M.T., Koehier F. and Sheriff R.E.; 1977: *Complex seismic trace analysis*. Geophys., **44**, 1041-1063, doi: 10.1190/1.1440994.

Urban T.M., Leon J.F., Manning S.W. and Fisher K.D.; 2014: *High resolution GPR detection of late Bronze Age architecture Kalavasos - Ayios Dhimitrios, Cyprus*. J. Appl. Geophys., **107**, 129-136, doi: 10.1016/j.jappgeo.2014.05.020.

Vohs A.B.; 2016: *3D seismic attributes analysis in reservoir characterization: the Morrison NE Field & Morrison Field, Clark County, Kansas*. M.Sc. Thesis in Geology, University of Kansas, Manhattan, KS, USA, 91 pp.

Zhao W., Tian G., Wang B., Shi Z. and Lin J.; 2012: *Application of 3D GPR attribute technology in archaeological investigations*. Appl. Geophys., **9**, 261-269, doi: 10.1007/s11770-012-0336-2.

Zhao W., Forte E., Pipan M. and Tian G.; 2013: *Ground penetrating radar (GPR) attribute analysis for archaeological prospection*. J. Appl. Geophys., **97**, 107-117, doi: 10.1016/j.jappgeo.2013.04.010.

Corresponding author: Zaidoon Taha Abdulrazzaq
                            Ministry of Science and Technology
                            Jamia Street, Baghdad, Al Jadriya, Iraq
                            Phone: +964 772 4614940; e-mail: zaidoon.taha@live.com